

Structural Transitions in Vortex Systems with Anisotropic Interactions

M.W. Olszewski,^{1,2} M. R. Eskildsen,² C. Reichhardt,¹ and C.J.O. Reichhardt¹

¹*Theoretical Division, Los Alamos National Laboratory, Los Alamos, New Mexico 87545 USA*

²*Department of Physics, University of Notre Dame, Notre Dame, Indiana 46656, USA*

(Dated: November 5, 2021)

We introduce a model of vortices in type-II superconductors with a four-fold anisotropy in the vortex-vortex interaction potential. Using numerical simulations we show that the vortex lattice undergoes structural transitions as the anisotropy is increased, with a triangular lattice at low anisotropy, a rhombic intermediate state, and a square lattice for high anisotropy. In some cases we observe a multi- q state consisting of an Archimedean tiling that combines square and triangular local ordering. At very high anisotropy, domains of vortex chain states appear. We discuss how this model can be generalized to higher order anisotropy as well as its applicability to other particle-based systems with anisotropic particle-particle interactions.

I. INTRODUCTION

A type-II superconductor subjected to a magnetic field forms vortices that each carry one quantum of magnetic flux. Due to their mutual repulsion, these vortices arrange themselves in an ordered vortex lattice (VL) the vortex-vortex interactions dominate external influences such as pinning by impurities or thermal disordering. The VL is triangular in isotropic superconductors¹; however, anisotropy in the vortex-vortex interactions can cause changes in the VL symmetry.² One of the most studied systems exhibiting a transition to a square VL is borocarbide materials^{3–10}. Transitions to square lattices have also been observed in high temperature superconductors,^{11–14} heavy fermion materials,^{15–18} and spin triplet superconductors such as Sr₂RuO₄.^{19–21} Additionally, transitions from triangular to square VLs can arise in other superfluid systems including Bose-Einstein condensates²² and dense nuclear matter in extreme conditions.²³

In superconducting systems, theoretical approaches used to study the VL structural transitions include modifications to the London model^{24,25}, addition of four-fold symmetric terms to the Ginzburg-Landau free energy²⁶, Eilenberger theory²⁷, modified Ginzburg-Landau approaches²⁸, and modifications to the vortex interactions produced by strain fields²⁹. Notably absent from this list are molecular dynamics (MD) simulations, which treat the vortices as point particles with bulk Bessel function interactions or thin film Pearl interactions. Until now, MD methods have only been applied to isotropic pairwise potentials, which produce a triangular VL in clean systems^{30–40}. One of the issues is that simply adding a stronger radial repulsive force along certain directions does not capture the triangular to square transitions in the vortex system. Instead, it is essential to consider the full anisotropic potential in which nonradial forces also arise. In addition to the equilibrium VL configurations, MD simulations give access to the statics and dynamics of a large number of vortices over long times.

Here we introduce a model for vortices in anisotropic

superconductors where the vortex-vortex interaction potential is extended to include a fourfold anisotropy. Using MD simulations we show that as the anisotropy is increased, the VL symmetry changes from triangular to rhombic to square. Additionally, in some cases we find a multi- q lattice state consisting of an Archimedean tiling with a combination of square and triangular local ordering. For very large anisotropy, domains of vortex chains appear. Our model can be generalized to any anisotropy and provides a basis for modeling VL reorientation or other vortex symmetry transitions such as those observed in multigap superconductors.⁴¹ The model can be applied not only to vortices in type-II superconductors, but also to other particle-based systems with anisotropic interactions where triangular to square transitions can arise. These include skyrmion lattices, where triangular to square transitions have recently been observed,^{42,43} as well as colloidal particles with anisotropic interactions.^{44,45}

II. MODEL

In an isotropic bulk superconductor, the vortex-vortex interaction potential is typically isotropically repulsive and takes the form of a zeroth order Bessel function, $U(r) = K_0(r)$.⁴⁶ For anisotropic materials, we propose the following modified pair potential for the vortex interactions:

$$U(r) = A_v K_0(r) \left[1 + A_a \cos^2 \left(\frac{n_a(\theta - \phi)}{2} \right) \right] \quad (1)$$

where $r = |\mathbf{r}_i - \mathbf{r}_j|$ is the distance between two vortices at positions \mathbf{r}_i and \mathbf{r}_j . The angle between the two vortices with respect to the positive x axis is given by $\theta = \tan^{-1}(r_y/r_x)$ where $\mathbf{r} = \mathbf{r}_i - \mathbf{r}_j$, $r_x = \mathbf{r} \cdot \hat{\mathbf{x}}$, and $r_y = \mathbf{r} \cdot \hat{\mathbf{y}}$. The rotation angle of the anisotropic axes is defined to be ϕ , and n_a is the order of the anisotropic interaction. The prefactor A_v represents the strength of the isotropic component of the vortex-vortex pair interaction force, and A_a controls the amplitude of the anisotropic interaction.

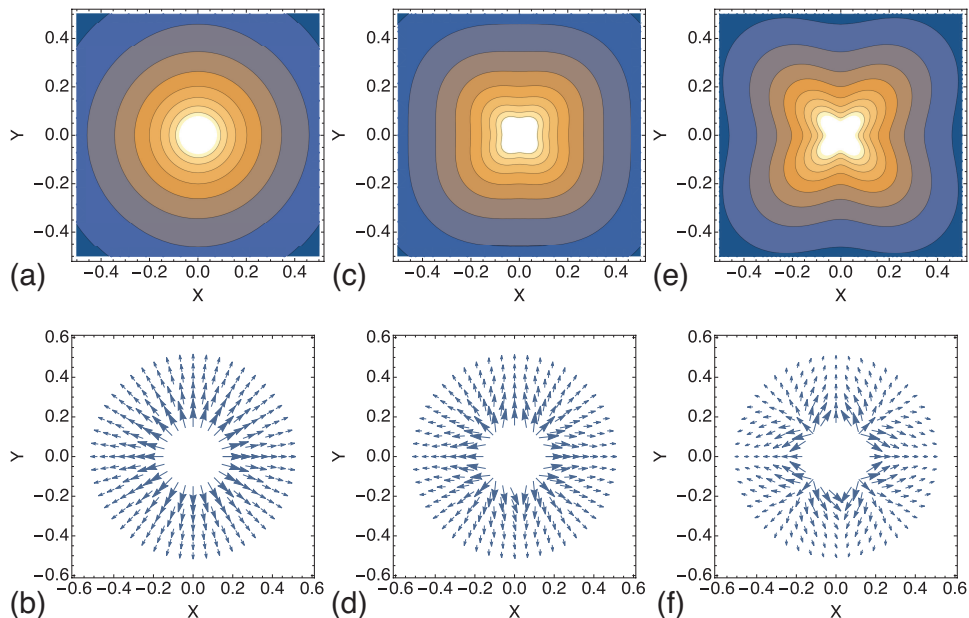


FIG. 1: Equipotential lines (a,c,e) and force fields (b,d,f) for the vortex-vortex interaction potential in Eq. 1 with $n_a = 4$ and $\phi = 45^\circ$. (a,b) Isotropic case with anisotropy strength $A_a = 0$. (c,d) At $A_a = 0.1$, nonradial forces begin to appear. (e,f) At $A_a = 0.25$ the nonradial forces are stronger.

To fully understand the manner in which Eq. (1) produces nonradial interactions, we examine the nature of the anisotropic forces generated by $U(r)$. For nonzero values of A_a , the potential is stronger along certain interaction directions and weaker between these directions. The anisotropic order n_a determines the number of strong interaction directions, which are evenly spaced in θ . For example, for $n_a = 6$ and $\phi = 0$, the interaction po-

tential passes through local maxima at $\theta = 0^\circ, 60^\circ, 120^\circ, 180^\circ, 240^\circ,$ and 300° . Setting $\phi = 15^\circ$, the local maxima of the interaction potential are shifted to $\theta = 15^\circ, 75^\circ, 135^\circ, 195^\circ, 255^\circ,$ and 315° . Between these values of θ , the interaction strength varies as a cosine. The force field from the potential is $\mathbf{F}_{vv} = -\nabla U = (-\frac{\partial U}{\partial x}, -\frac{\partial U}{\partial y})$ with components

$$F_x = A_v \left[\cos(\theta) K_1(r) \left(1 + A_a \cos^2 \left(\frac{n_a(\theta - \phi)}{2} \right) \right) - \frac{\sin(\theta)}{r} K_0(r) \frac{n_a A_a}{2} \sin(n_a(\theta - \phi)) \right] \quad (2)$$

$$F_y = A_v \left[\sin(\theta) K_1(r) \left(1 + A_a \cos^2 \left(\frac{n_a(\theta - \phi)}{2} \right) \right) + \frac{\cos(\theta)}{r} K_0(r) \frac{n_a A_a}{2} \sin(n_a(\theta - \phi)) \right]. \quad (3)$$

In the present work we focus on the $n_a = 4$ interaction potential with fourfold anisotropy; however, by changing n_a our model can be applied to twofold ($n_a = 2$), sixfold ($n_a = 6$), or other degrees of anisotropy. In Fig. 1(a,b) we plot the equipotential lines and force field for $U(r)$ from Eq. 1 for the isotropic case with $A_a = 0$, where the equipotential lines are circularly symmetric and the forces are strictly radial. At $A_a = 0.1$ in Fig. 1(c,d), the fourfold symmetry is apparent and weak nonradial forces appear. In Fig. 1(e,f) at $A_a = 0.25$, the fourfold symmetry is much more pronounced and the nonradial forces are clearly visible.

To investigate the VL ground states that emerge as

the anisotropy of the potential increases, we perform MD simulations of $N = 441$ vortices in a two-dimensional system of size $L \times L$ with $L = 36\lambda$ and periodic boundary conditions in the x and y directions. Distances are measured in units of the London penetration depth λ . The dynamics of vortex i is governed by an overdamped equation of motion:

$$\eta \frac{d\mathbf{r}_i}{dt} = \mathbf{F}_{vv}^i + \mathbf{F}_T^i. \quad (4)$$

Here η is the damping constant which we set equal to unity. Thermal forces are modeled by Langevin kicks \mathbf{F}_T^i which have the properties $\langle \mathbf{F}_T \rangle = 0.0$ and

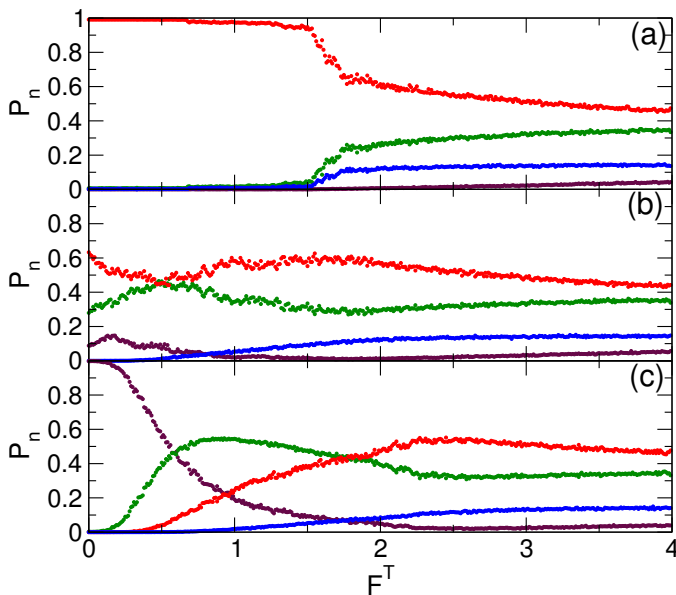


FIG. 2: Measures P_n of VL ordering versus temperature F^T during the annealing procedure for P_7 (blue), P_6 (red), P_5 (green), and P_4 (maroon) in samples with $A_v = 2.0$. (a) In the isotropic system with $A_a = 0$, the vortices form a triangular lattice with $P_6 = 1.0$. (b) For $A_a = 0.039$, rhombic ordering appears. (d) At $A_a = 0.099$, the vortices form a square lattice with $P_4 = 1.0$.

$\langle \mathbf{F}_T^i(t) \mathbf{F}_T^j(t') \rangle = 2\eta k_B T \delta_{ij} \delta(t-t')$ where k_B is the Boltzmann constant. We perform simulated annealing by starting in a high temperature molten state and gradually cooling the system to $T = 0$. We use an initial temperature of $F^T = 4.0$ and decrement the temperature by $\Delta F^T = -0.01$ every 40,000 simulation time steps, which is long enough to ensure that the system reaches an equilibrium state.

III. VORTEX STRUCTURES

We use a Voronoi construction to obtain the local coordination number z_i of each vortex, and compute the fraction P_n of vortices with coordination number n using $P_n = N^{-1} \sum_{i=1}^N \delta(z_i - n)$ for $n = 4, 5, 6$, and 7 . Figure 2(a) shows P_4 , P_5 , P_6 , and P_7 versus F^T obtained during the annealing process in an isotropic system with $A_a = 0$ and $A_v = 2.0$. Initially the system is in a high temperature molten state, and as F^T is reduced the vortices order into a triangular lattice with $P_6 = 1.0$. In Fig. 2(b) at $A_a = 0.039$, the vortices freeze into a state with rhombic ordering, while in Fig. 2(c) at $A_a = 0.099$, the vortices form a square lattice with $P_4 = 1.0$. Together, these results show how the equilibrium ($T = 0$) value of P_6 is suppressed and the value of P_4 grows as the anisotropy is increased. Compared to the drop in P_6 , the rise of P_4 is more gradual and happens at a lower F^T .

We can further characterize the final $F^T = 0$ state us-

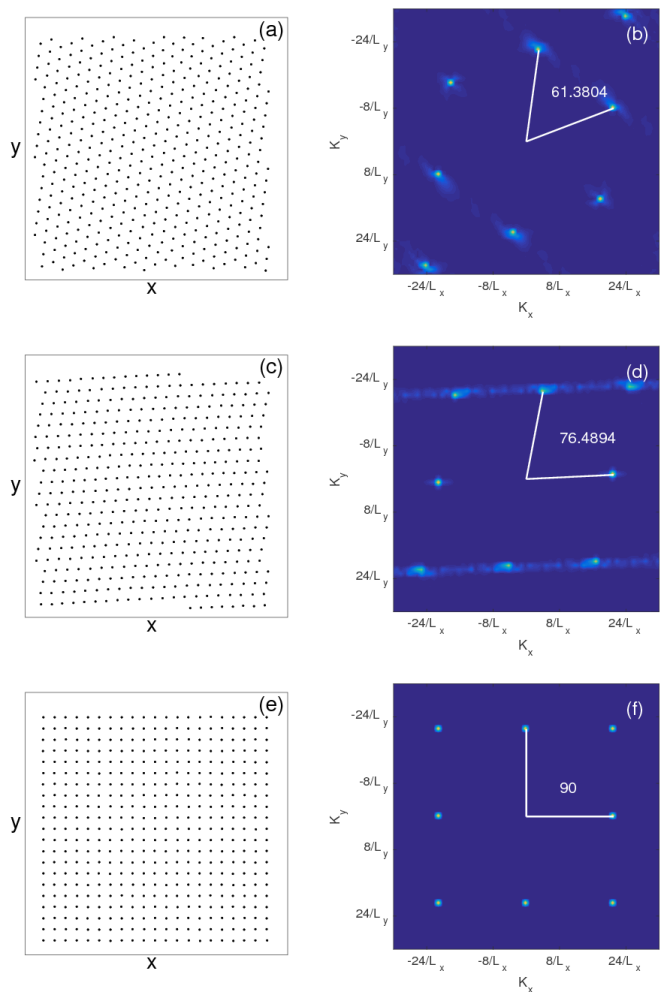


FIG. 3: Real space VL configurations (a,c,e) and corresponding heightfield plots of the structure factor $|S(\mathbf{k})|$ (b,d,f) after annealing in samples with $A_v = 2.0$. (a,b) The isotropic system with $A_a = 0$ has triangular ordering and a lattice angle θ_l (marked in white) of $\theta_l \approx 60^\circ$. (c,d) At $A_a = 0.039$, the vortices form a rhombic lattice with $\theta_l \approx 76^\circ$. (e,f) At $A_a = 0.099$, the vortices form a square lattice with $\theta_l = 90^\circ$.

ing the structure factor $S(\mathbf{k}) = N^{-1} |\sum_i^N \exp(-i\mathbf{k} \cdot \mathbf{r}_i)|^2$. In Fig. 3(a) we illustrate the final real space vortex positions in a sample with $A_a = 0$ and $A_v = 2.0$, and in Fig. 3(b) we plot the corresponding $|S(\mathbf{k})|$ as a heightfield. The lattice angle θ_l is defined to be the angle between adjacent first-order peaks in $|S(\mathbf{k})|$, as illustrated in Fig. 3(b), and for the $A_a = 0$ triangular lattice, $\theta_l \approx 60^\circ$. The triangular lattice is slightly distorted by our perfectly square simulation box, which gives us the minor deviation from the ideal value $\theta_l = 60^\circ$. In Fig. 3(c,d), at $A_a = 0.039$ the vortices form a rhombic lattice with $\theta_l \approx 76^\circ$. At $A_a = 0.099$ in Fig. 3(e,f), a square lattice appears with $\theta_l = 90^\circ$. In Fig. 4 we plot the lattice angle θ_l versus A_a for samples with $A_v = 1.0, 1.5, 2.0$, and 2.5 . In all cases, at low $A_a \lesssim 0.3$ the vortex ordering is triangular, at intermediate A_a a rhombic lat-

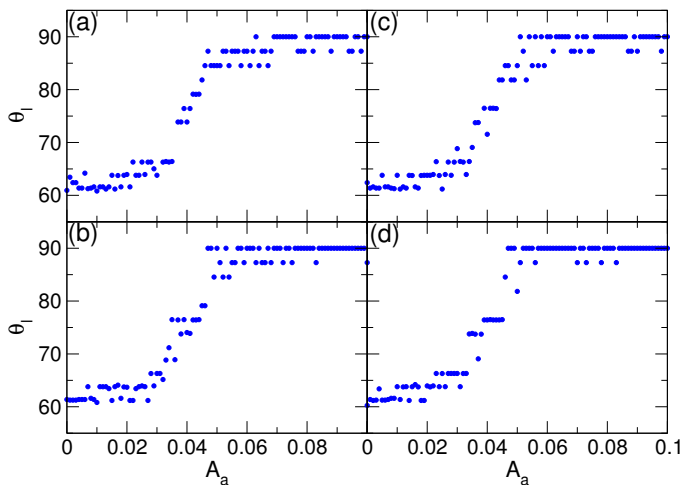


FIG. 4: Lattice angle θ_l versus A_a for systems with (a) $A_v = 1.0$, (b) $A_v = 1.5$, (c) $A_v = 2.0$, and (d) $A_v = 2.5$. In all cases, the vortices form a triangular VL at small A_a with $\theta_l \approx 60^\circ$, pass through an intermediate rhombic state with $\theta_l \approx 75^\circ$, and then form a square lattice with $\theta_l \approx 90^\circ$ at large A_a .

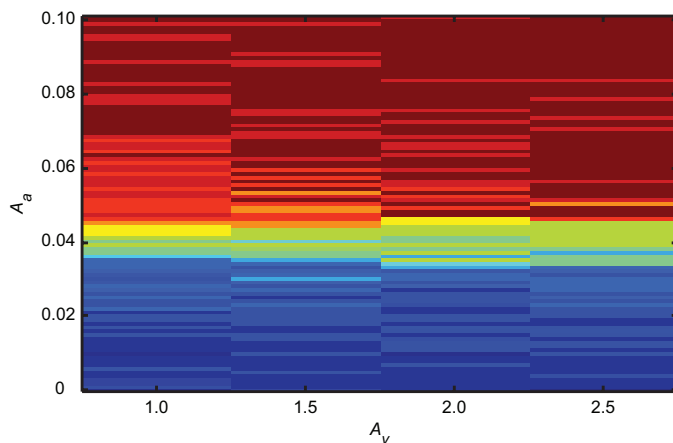


FIG. 5: Lattice ordering phase diagram as a function of A_a versus A_v . Blue: triangular order; red: square order; yellow and green shades: rhombic order, which is centered around $A_a = 0.04$.

tice structure appears, and at large $A_a \gtrsim 0.5$ a square VL emerges. In Fig. 5 we plot a structural phase diagram indicating where the triangular, rhombic, and square VLs appear as a function of A_a versus A_v . The evolution of the VL symmetry is nearly independent of the value of A_v , showing that the triangular-to-square transition is a robust feature of our MD simulations.

For some combinations of A_a and A_v what we term a multi- q state appears in which the vortices exhibit simultaneous square and triangular ordering. Figure 6 shows both the real space Voronoi polygons and the corresponding $|S(\mathbf{k})|$ for multi- q states in samples with $A_a = 0.04$. For both $A_v = 2.0$ in Fig. 6(a,b) and $A_v = 2.8$ in Fig. 6(c,d) we find the same combination of square

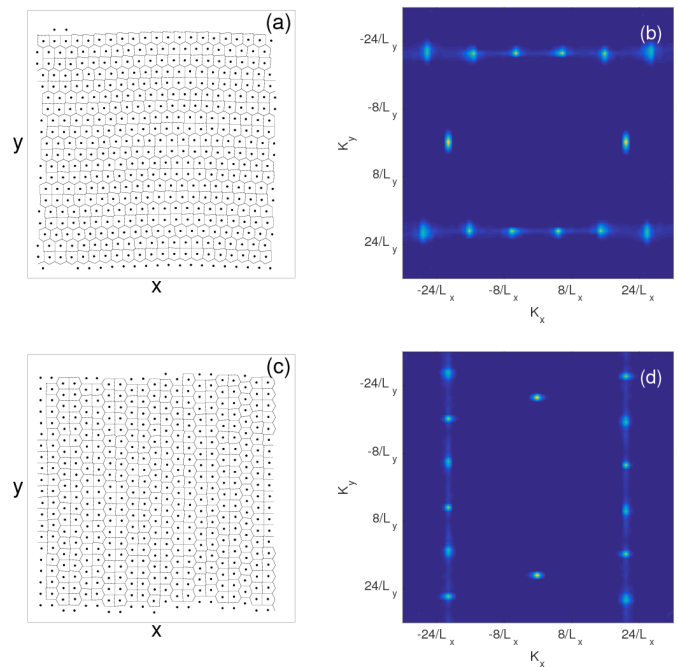


FIG. 6: Multi- q Voronoi constructions for the real space vortex positions (a,c) and the corresponding structure factor $|S(\mathbf{k})|$ (b,d) in samples with $A_a = 0.04$ at $A_v = 2.0$ (a,b) and $A_v = 2.8$ (c,d). The Voronoi polygons indicate that there is a combination of square and triangular ordering in the form of an Archimedean tiling, producing multiple peaks in $|S(\mathbf{k})|$.

and triangular ordering in the Voronoi polygons, while $|S(\mathbf{k})|$ exhibits multiple sets of peaks. As illustrated in Fig. 6, the multi- q ordering can be oriented along either the x or the y direction. The multi- q VL structure closely resembles an Archimedean tiling in which space is filled with a combination of square and triangular tiles.⁴⁷ Archimedean ordering of this type has also been observed for colloidal assemblies driven over quasiperiodic substrates, where it arises due to the competition between the ordering imposed by the substrate and the triangular ordering that minimizes the colloid-colloid interaction energy.^{48,49} In our system the competition responsible for producing this structure is between the square and triangular orderings favored by the anisotropy. We note that the multi- q state only appears occasionally in regions of A_a and A_v that are dominated by the rhombic state, suggesting that it could be metastable. Additionally, the two different orientations of the multi- q state that we find indicate that in diffraction experiments on macroscopic samples, domains of different orientations will most likely coexist. This would smear out the peaks in $|S(\mathbf{k})|$, making it difficult to deconvolute the signal from an individual domain orientation. As a result, local probe imaging techniques may be the best method for observing multi- q states.

For anisotropies A_a larger than those discussed above, we find that the square lattice gradually transforms into domains of vortex chains. This process is illustrated in

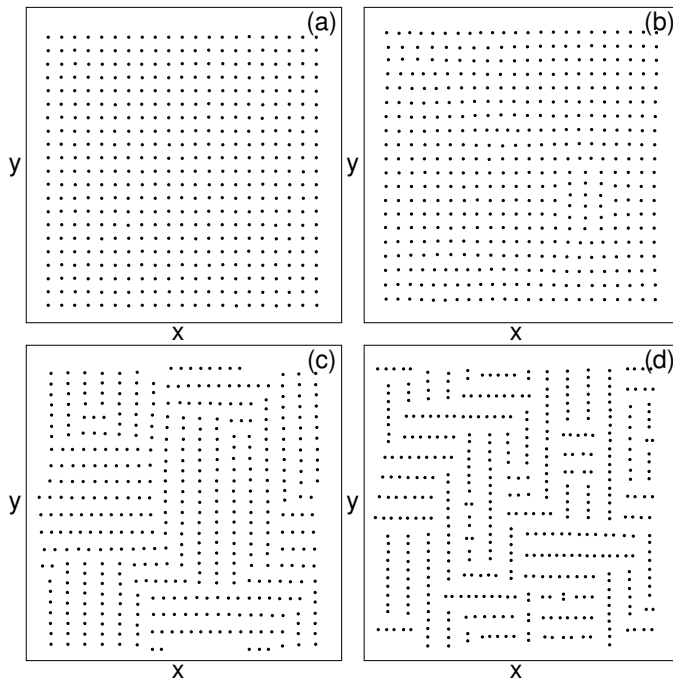


FIG. 7: Real space vortex configurations showing the emergence of chain states in systems with $A_v = 2.0$. At $A_a = 0.1$ (a) the VL is square. For $A_a = 0.6$ (b) the square lattice develops some local distortions and dislocations. At $A_a = 1.3$ (c) chain state domains appear, and these become more pronounced for $A_a = 3.0$ (d).

Fig. 7 for systems with $A_v = 2.0$ where A_a is increased from $A_a = 0.1$ to $A_a = 3.0$. Although such levels of anisotropy may seem unphysically large, there have been several observations of vortex chain states, including domains of chains in different borocarbides and in Sr_2RuO_4 at low fields.^{50–52} While these observations are typically attributed to an attractive interaction between vortices at intermediate range, it may still be possible to model

these chain states by introducing strongly anisotropic vortex-vortex interactions.

IV. SUMMARY

We have introduced a model for vortices with anisotropic pairwise interactions, focusing on the case of four-fold asymmetry. Using MD simulations we show that this model captures a transition from a triangular lattice at low anisotropy to a square VL at high anisotropy, with an intermediate rhombic phase. We also find that in some cases a multi- q state with Archimedean ordering appears in which the vortices have both square and triangular local ordering. For the highest anisotropy values, domains of vortex chains form. Our model could be applied to study the dynamics near the VL transitions, where nonequilibrium phenomena can arise.^{53,54} Additionally, it can be generalized for higher order anisotropy in order to capture other types of symmetry and reorientation transitions in VLs.^{55–59} It is also possible to use the model with different isotropic pairwise interactions to investigate hexagonal to square transitions in other particle-based systems, such as skyrmions or colloids with anisotropic interactions.

Acknowledgments

We are grateful to D. Green, M. Lamichhane, X. Ma, D. McDermott and K. Newman for assistance and discussions. This research was supported in part by the Notre Dame Center for Research Computing. M.R.E. was supported by the U.S. Department of Energy, Office of Basic Energy Sciences, under Award No. DE-SC0005051. This work was carried out under the auspices of the NNSA of the U.S. DoE at LANL under Contract No. DE-AC52-06NA25396.

¹ W.H. Kleiner, L.M. Roth, and S. H. Autler, Bulk solution of Ginzburg-Landau equations for type II superconductors: upper critical field region, *Phys. Rev.* **133**, A1226 (1964).

² J. Schelten in *Anisotropic Effects in Superconductors*, ed. H. Webger (Plenum, New York, 1977).

³ U. Yaron, P.L. Gammel, A.P. Ramirez, D.A. Huse, D.J. Bishop, A.I. Goldman, C. Stassis, P.C. Canfield, K. Mortensen, and M.R. Eskildsen, Microscopic coexistence of magnetism and superconductivity in $\text{ErNi}_2\text{B}_2\text{C}$, *Nature* **382**, 236 (1996).

⁴ M.R. Eskildsen, P.L. Gammel, B.P. Barber, A.P. Ramirez, D.J. Bishop, N.H. Andersen, K. Mortensen, C.A. Bolle, C.M. Lieber, and P.C. Canfield, Structural stability of the square flux line lattice in $\text{YNi}_2\text{B}_2\text{C}$ and $\text{LuNi}_2\text{B}_2\text{C}$ studied with small angle neutron scattering, *Phys. Rev. Lett.* **79**, 487 (1997).

⁵ Y. De Wilde, M. Iavarone, U. Welp, V. Metlushko, A.E.

Koshelev, I. Aranson, G.W. Crabtree, and P.C. Canfield, Scanning tunneling microscopy observation of a square Abrikosov lattice in $\text{LuNi}_2\text{B}_2\text{C}$, *Phys. Rev. Lett.* **78**, 4273 (1997).

⁶ M.R. Eskildsen, A.B. Abrahamsen, V.G. Kogan, P.L. Gammel, K. Mortensen, N.H. Andersen, and P.C. Canfield, Temperature dependence of the flux line lattice transition into square symmetry in superconducting $\text{LuNi}_2\text{B}_2\text{C}$, *Phys. Rev. Lett.* **86**, 5148 (2001).

⁷ M.R. Eskildsen, A.B. Abrahamsen, D. López, P.L. Gammel, D.J. Bishop, N.H. Andersen, K. Mortensen, and P.C. Canfield, Flux line lattice reorientation in the borocarbide superconductors with $H_{||}a$, *Phys. Rev. Lett.* **86**, 320 (2001).

⁸ M.R. Eskildsen, P.L. Gammel, B.P. Barber, U. Yaron, A.P. Ramirez, D.A. Huse, D.J. Bishop, C. Bolle, C.M. Lieber, S. Oxx, S. Sridhar, N.H. Andersen, K. Mortensen, and P.C.

- Canfield, Observation of a field-driven structural phase transition in the flux line lattice in $\text{ErNi}_2\text{B}_2\text{C}$, *Phys. Rev. Lett.* **78**, 1968 (1997).
- ⁹ H. Sakata, M. Oosawa, K. Matsuba, N. Nishida, H. Takeya, and K. Hirata, Imaging of a vortex lattice transition in $\text{YNi}_2\text{B}_2\text{C}$ by scanning tunneling spectroscopy, *Phys. Rev. Lett.* **84**, 1583 (2000).
- ¹⁰ C.D. Dewhurst, S.J. Levett, and D.McK. Paul, Vortex-lattice symmetry near T_c in $\text{YNi}_2\text{B}_2\text{C}$, *Phys. Rev. B* **72**, 014542 (2005).
- ¹¹ M.R. Eskildsen, Vortex lattices in type-II superconductors studied by small-angle neutron scattering, *Front. Phys.* **6**, 398 (2011).
- ¹² R. Gilardi, J. Mesot, A. Drew, U. Divakar, S.L. Lee, E.M. Forgan, O. Zaharko, K. Conder, V.K. Aswal, C.D. Dewhurst, R. Cubitt, N. Momono, and M. Oda, Direct evidence for an intrinsic square vortex lattice in the overdoped high- T_c superconductor $\text{La}_{1.83}\text{Sr}_{0.17}\text{CuO}_{4+\delta}$, *Phys. Rev. Lett.* **88**, 217003 (2002).
- ¹³ S.P. Brown, D. Charalambous, E.C. Jones, E.M. Forgan, P.G. Kealey, A. Erb, and J. Kohlbrecher, Triangular to square flux lattice phase transition in $\text{YBa}_2\text{Cu}_3\text{O}_7$, *Phys. Rev. Lett.* **92**, 067004 (2004).
- ¹⁴ A.S. Cameron, J.S. White, A.T. Holmes, E. Blackburn, E.M. Forgan, R. Riyat, T. Loew, C.D. Dewhurst, and A. Erb, High magnetic field studies of the vortex lattice structure in $\text{YBa}_2\text{Cu}_3\text{O}_7$, *Phys. Rev. B* **90**, 054502 (2014).
- ¹⁵ M.R. Eskildsen, C.D. Dewhurst, B.W. Hoogenboom, C. Petrovic, and P.C. Canfield, Heavy fermion hexagonal and square flux line lattices in CeCoIn_5 , *Phys. Rev. Lett.* **90**, 187001 (2003).
- ¹⁶ L. DeBeer-Schmitt, C.D. Dewhurst, B.W. Hoogenboom, C. Petrovic, and M.R. Eskildsen, Field dependent coherence length in the superclean, high- κ superconductor CeCoIn_5 , *Phys. Rev. Lett.* **97**, 127001 (2006).
- ¹⁷ A.D. Bianchi, M. Kenzelmann, L. DeBeer-Schmitt, J.S. White, E.M. Forgan, J. Mesot, M. Zolliker, J. Kohlbrecher, R. Movshovich, E.D. Bauer, J.L. Sarrao, Z. Fisk, C. Petrovic, and M.R. Eskildsen, Superconducting vortices in CeCoIn_5 : Toward the Pauli-limiting field, *Science* **319**, 177 (2008).
- ¹⁸ J.S. White, P. Das, M.R. Eskildsen, L. DeBeer-Schmitt, E.M. Forgan, A.D. Bianchi, M. Kenzelmann, M. Zolliker, S. Gerber, J.L. Gavilano, J. Mesot, R. Movshovich, E.D. Bauer, J.L. Sarrao, and C. Petrovic, Observations of Pauli paramagnetic effects on the flux line lattice in CeCoIn_5 , *New J. Phys.* **12**, 023026 (2010).
- ¹⁹ T.M. Riseman, P.G. Kealey, E.M. Forgan, A.P. Mackenzie, L.M. Galvin, A.W. Tyler, S.L. Lee, C. Ager, D.M. Paul, C.M. Aegerter, R. Cubitt, Z.Q. Mao, T. Akima, and Y. Maeno, Observation of a square flux-line lattice in the unconventional superconductor Sr_2RuO_4 , *Nature (London)* **396**, 242 (1998).
- ²⁰ P.J. Curran, V.V. Khotkevych, S.J. Bending, A.S. Gibbs, S.L. Lee, and A.P. Mackenzie, Vortex imaging and vortex lattice transitions in superconducting Sr_2RuO_4 single crystals, *Phys. Rev. B* **84**, 104507 (2011).
- ²¹ S.J. Ray, A.S. Gibbs, S.J. Bending, P.J. Curran, E. Babaev, C. Baines, A.P. Mackenzie, and S.L. Lee, Muon-spin rotation measurements of the vortex state in Sr_2RuO_4 : Type-1.5 superconductivity, vortex clustering, and a crossover from a triangular to a square vortex lattice, *Phys. Rev. B* **89**, 094504 (2014).
- ²² V. Schweikhard, I. Coddington, P. Engels, S. Tung, and E.A. Cornell, Vortex-lattice dynamics in rotating spinor Bose-Einstein condensates, *Phys. Rev. Lett.* **93**, 210403 (2004).
- ²³ M.N. Chernodub, J. Van Doorselaere, and H. Verschelde, Electromagnetically superconducting phase of the vacuum in a strong magnetic field: Structure of superconductor and superfluid vortex lattices in the ground state, *Phys. Rev. D* **85**, 045002 (2012).
- ²⁴ V.G. Kogan, M. Bullock, B. Harmon, P. Miranovic, Lj. Dobrosavljevic-Grujic, P.L. Gammel, and D. J. Bishop, Vortex lattice transitions in borocarbides, *Phys. Rev. B* **55**, R8693(R)(1997).
- ²⁵ M. Franz, I. Affleck, and M. Amin, Theory of Equilibrium Flux Lattices in Unconventional Superconductors, *Phys. Rev. Lett.* **79**, 1555 (1997).
- ²⁶ K. Park and D.A. Huse, Phase transition to a square vortex lattice in type-II superconductors with fourfold anisotropy, *Phys. Rev. B* **58**, 9427 (1998).
- ²⁷ N. Nakai, P. Miranovic, M. Ichioka, and K. Machida, Reentrant vortex lattice transformation in fourfold symmetric superconductors, *Phys. Rev. Lett.* **89**, 237004 (2002).
- ²⁸ A.D. Klironomos and A.T. Dorsey, Vortex lattice structural transitions: a Ginzburg-Landau model approach, *Phys. Rev. Lett.* **91**, 097002 (2003).
- ²⁹ S.-Z. Lin and V.G. Kogan, Strain-induced intervortex interaction and vortex lattices in tetragonal superconductors, *Phys. Rev. B* **95**, 054511 (2017).
- ³⁰ E.H. Brandt, Computer simulation of flux pinning in type-II superconductors, *Phys. Rev. Lett.* **50**, 1599 (1983).
- ³¹ H.J. Jensen, A. Brass, Y. Brechet, and A.J. Berlinsky, Current-voltage characteristics in a two-dimensional model for flux flow in type-II superconductors, *Phys. Rev. B* **38**, 9235 (1988).
- ³² A.E. Koshelev and V.M. Vinokur, Dynamic melting of the vortex lattice, *Phys. Rev. Lett.* **73**, 3580 (1994).
- ³³ C.J. Olson, C. Reichhardt, and F. Nori, Nonequilibrium dynamic phase diagram for vortex lattices, *Phys. Rev. Lett.* **81**, 3757 (1998).
- ³⁴ A. Kolton, D. Domínguez, and N. Grønbech-Jensen, Hall noise and transverse freezing in driven vortex lattices, *Phys. Rev. Lett.* **83**, 3061 (1999).
- ³⁵ Q.H. Chen, G. Teniers, B.B. Jin, and V.V. Moshchalkov, Pinning properties and vortex dynamics in thin superconducting films with ferromagnetic and antiferromagnetic arrays of magnetic dots, *Phys. Rev. B* **73**, 014506 (2006).
- ³⁶ C. Reichhardt and C.J.O. Reichhardt, Transport anisotropy as a probe of the interstitial vortex state in superconductors with artificial pinning arrays, *Phys. Rev. B* **79**, 134501 (2009).
- ³⁷ D. Ray, C. Reichhardt, and C.J.O. Reichhardt, Pinning, ordering, and dynamics of vortices in conformal crystal and gradient pinning arrays, *Phys. Rev. B* **90**, 094502 (2014).
- ³⁸ Q. Le Thien, D. McDermott, C.J.O. Reichhardt, and C. Reichhardt, Orientational ordering, buckling, and dynamic transitions for vortices interacting with a periodic quasi-one-dimensional substrate, *Phys. Rev. B* **93**, 014504 (2016).
- ³⁹ H.J. Zhao, W. Wu, W. Zhou, Z.X. Shi, V.R. Misko, and F.M. Peeters, Reentrant dynamics of driven pancake vortices in layered superconductors, *Phys. Rev. B* **94**, 024514 (2016).
- ⁴⁰ R.M. Menezes and C.C. de Souza Silva, Conformal vortex crystals, arXiv:1703.07739.
- ⁴¹ R. Cubitt, M.R. Eskildsen, C.D. Dewhurst, J. Jun, S.M.

- Kazakov, and J. Karpinski, Effects of two-band superconductivity on the flux-line lattice in magnesium diboride, *Phys. Rev. Lett.* **91**, 047002 (2003).
- ⁴² K. Karube, J.S. White, N. Reynolds, J.L. Gavilano, H. Oike, A. Kikkawa, F. Kagawa, Y. Tokunaga, H.M. Rønnow, Y. Tokura, and Y. Taguchi, Robust metastable skyrmions and their triangular-square lattice structural transition in a high-temperature chiral magnet, *Nature Mater.* **15**, 1237 (2016).
- ⁴³ T. Nakajima, H. Oike, A. Kikkawa, E.P. Gilbert, N. Booth, K. Kakurai, Y. Taguchi, Y. Tokura, F. Kagawa, and T. Arima, Skyrmion lattice structural transition in MnSi, *Sci. Adv.* **3**, 1602562 (2017).
- ⁴⁴ C. Eisenmann, U. Gasser, P. Keim, and G. Maret, Anisotropic defect-mediated melting of two-dimensional colloidal crystals, *Phys. Rev. Lett.* **93**, 105702 (2004).
- ⁴⁵ S.C. Glotzer and M.J. Solomon, Anisotropy of building blocks and their assembly into complex structures, *Nature Mater.* **6**, 557 (2007).
- ⁴⁶ M. Tinkham, *Introduction to Superconductivity: Second Edition* (McGraw-Hill, New York, 1996).
- ⁴⁷ P. Pearce, *Structure in Nature is a Strategy for Design* (MIT Press, Cambridge, MA, 1978).
- ⁴⁸ J. Mikhael, J. Roth, L. Helden, and C. Bechinger, Archimedean-like tiling on decagonal quasicrystalline surfaces, *Nature (London)* **454**, 501 (2008).
- ⁴⁹ M. Schmiedeberg, M.S. Rausch, J. Roth, L. Helden, C. Bechinger, and H. Stark, Archimedean-like colloidal tilings on substrates with decagonal and tetradecagonal symmetry, *Eur. Phys. J. E* **32**, 25 (2010).
- ⁵⁰ L.Ya. Vinnikov, J. Anderegg, S.L. Bud'ko, P.C. Canfield, and V.G. Kogan, Domain structure in $\text{ErNi}_2\text{B}_2\text{C}$ and $\text{HoNi}_2\text{B}_2\text{C}$ single crystals observed by a high-resolution Bitter decoration technique, *Phys. Rev. B* **71**, 224513 (2005).
- ⁵¹ V.O. Dolocan, C. Veauvy, F. Servant, P. Lejay, K. Hasselbach, Y. Liu, and D. Mailly, Observation of vortex coalescence in the anisotropic spin-triplet superconductor Sr_2RuO_4 , *Phys. Rev. Lett.* **95**, 097004 (2005).
- ⁵² P.J. Curran, V.V. Khotkevych, S.J. Bending, A.S. Gibbs, S.L. Lee, and A.P. Mackenzie, Vortex imaging and vortex lattice transitions in superconducting Sr_2RuO_4 single crystals, *Phys. Rev. B* **84**, 104507 (2011).
- ⁵³ B. Rosenstein and A. Knigavko, Anisotropic peak effect due to structural phase transition in the vortex lattice, *Phys. Rev. Lett.* **83**, 844 (1999).
- ⁵⁴ A.K. Pramanik, L. Harnagea, C. Nacke, A.U.B. Wolter, S. Wurmehl, V. Kataev, and B. Büchner, Fishtail effect and vortex dynamics in LiFeAs single crystals, *Phys. Rev. B* **83**, 094502 (2011).
- ⁵⁵ R. Cubitt, M.R. Eskildsen, C.D. Dewhurst, J. Jun, S.M. Kazakov, and J. Karpinski, Effects of two-band superconductivity on the flux-line lattice in magnesium diboride, *Phys. Rev. Lett.* **91**, 047002 (2003).
- ⁵⁶ M. Laver, E.M. Forgan, S.P. Brown, D. Charalambous, D. Fort, C. Bowell, S. Ramos, R.J. Lycett, D.K. Christen, J. Kohlbrecher, C.D. Dewhurst, and R. Cubitt, Spontaneous symmetry-breaking vortex lattice transitions in pure niobium, *Phys. Rev. Lett.* **96**, 167002 (2006).
- ⁵⁷ S. Mühlbauer, C. Pfleiderer, P. Böni, M. Laver, E.M. Forgan, D. Fort, U. Keiderling, and G. Behr, Morphology of the superconducting vortex lattice in ultrapure niobium, *Phys. Rev. Lett.* **102**, 136408 (2009).
- ⁵⁸ J.S. White, V. Hinkov, R.W. Heslop, R.J. Lycett, E.M. Forgan, C. Bowell, S. Strässle, A.B. Abrahamsen, M. Laver, C.D. Dewhurst, J. Kohlbrecher, J.L. Gavilano, J. Mesot, B. Keimer, and A. Erb, Fermi surface and order parameter driven vortex lattice structure transitions in twin-free $\text{YBa}_2\text{Cu}_3\text{O}_7$, *Phys. Rev. Lett.* **102**, 097001 (2009).
- ⁵⁹ P.K. Biswas, M.R. Lees, G. Balakrishnan, D.Q. Liao, D.S. Keeble, J.L. Gavilano, N. Egetenmeyer, C.D. Dewhurst, and D.McK. Paul, First-order reorientation transition of the flux-line lattice in CaAlSi , *Phys. Rev. Lett.* **108**, 077001 (2012).